FIRST-PRINCIPLES STUDY OF CALCIUM-BASED SULFUR FIXERS AND THEIR PRODUCTS

by

***Guoyan CHEN*[*], *Jianing CHEN, Anchao ZHANG*[*], *Haoxin DENG,
Yanyang MEI, Xiaoping WEN, Fahui WANG, Wei SHENG,
Zheng SHEN, and Shuangshuang ZUO***

School of Mechanical and Power Engineering, Henan Polytechnic University, Jiaozuo, China

Original scientific paper
https://doi.org/10.2298/TSCI210824350C

Calcium-based sulfur-fixing agent, as the main sulfur-fixing product, is widely used in power plant boiler systems. In order to further study the thermodynamic properties and reaction characteristics of calcium-based sulfur fixing agent and its products, the method of combining power plant experiment with theory was used. The electronic structure, thermodynamic properties and density of states of quicklime, limestone, calcium sulfate ($CaSO_4$) and calcium sulphoaluminate have been calculated based on the first-principles ultra-soft pseudopotential plane wave method of density functional theory. The generalized gradient approximation algorithm is used to optimize the structure of various minerals to achieve the most stable state. The results show that the enthalpy, entropy, specific heat capacity at constant pressure and Gibbs free energy of calcium sulfonate vary greatly from 25-1000 K, while the change of calcium oxide (CaO) is small, and that of calcium carbonate ($CaCO_3$) and $CaSO_4$ are between them. It shows that calcium sulphoaluminate has strong stability and more energy is needed to destroy the molecular structure of calcium sulphoaluminate. The CaO is the most unstable and requires less energy to react. The $CaCO_3$ and $CaSO_4$ are in between. The variation range of $CaSO_4$ is greater than that of $CaCO_3$, indicating that the stability of $CaSO_4$ is higher than that of $CaCO_3$. The experimental results show that the desulfurization efficiency of generating calcium sulphoaluminate is much higher than that of only generating $CaSO_4$, indicating that calcium sulphoaluminate is very stable, which is consistent with the calculated results.

Key words: *first principles, calcium-based sulfur-fixing agents, desulfurization, density functional theory*

Introduction

In response to the increasingly stringent requirements for environmental protection, both coal-fired boilers and coal-fired kilns are basically equipped with in-furnace sulfur fixation facilities or flue gas desulfurization devices. Circulating fluidized bed boiler is a typical furnace for sulfur fixation, mainly by injecting quicklime or limestone of suitable particle size into the furnace as a sulfur fixation agent, which reacts with sulfur oxides in the furnace to generate sulfur fixation products such as $CaSO_4$ [1-4]. The investment and operating costs of this method are both low, and it has been widely used. However, the limestone furnace decomposition and sulfur fixation technology have their own shortcomings [5-10]:

---

[*] Corresponding authors, e-mail: 254568182@qq.com; anchaozhang@126.com

- The decomposition time of limestone in the furnace is longer, and the organic sulfur volatilized in the coal is shorter, resulting in the decomposition of CaO and the decomposed sulfur. Oxides cannot match the reaction well, which affect the efficiency of sulfur fixation in the furnace, resulting in a large concentration of sulfur oxides in the flue gas.
- During the operation of the boiler, in order to increase the power generation, the load fluctuations will inevitably occur, causing the temperature in the furnace to rise more than 900 °C, resulting in the instability of the solid sulfide calcium sulfite and $CaSO_4$, which are decomposed into sulfur dioxide and sulfur trioxide enter the flue gas, reducing the desulfurization efficiency of the entire system. In addition, the local high temperature may cause the high temperature sintering the sulfur fixer and its common products, blocking the surface micropores of the desulfurizer, leading to the decrease of the specific surface area of the desulfurizer particles, affecting its reaction with sulfur oxides, and reducing the desulfurization efficiency [11-15].

In order to avoid the occurrence of the aforementioned situation, a composite mineralized sulfur-fixing agent with quicklime and Al_2O_3 as the main components is selected for the desulfurization reaction. Adding appropriate amount of alkali metals (ferric oxide, calcium fluoride) to the compound mineralized sulfur fixation agent, calcium fluoride and ferric oxide and calcium based sulfur fixation agent at high temperature can form a low melting point of solid-liquid phase eutectic, reduce the reaction temperature of the product, promote the formation of the reaction at a lower temperature [16]. In addition, the solid-liquid eutectic can promote the reformation of the calcium-based lattice structure, with more voids, larger pore size and more uniform distribution. In order to further study the change of micro-structure, the thermodynamic properties of calcium-based sulfur fixing agent and its products were analyzed by the first principles method [17-19]. The first principles method does not rely on empirical data, and takes the polyatomic system as a multiparticle system composed of electrons and nucleus. Starting from the basic laws of quantum mechanics, we can reasonably predict the properties of the microscopic system. In recent years, there have been many reports on the calculation of the electronic structure and thermodynamic properties of solids based on the first principles. It is the first time to study the structure model of inorganic minerals in sulfur-fixing agents. In this study, the structural optimization and thermodynamic properties calculation of $CaCO_3$, CaO, $CaSO_4$, and calcium sulfoaluminate are used to study the principle of sulfur fixation of calcium-based sulfur fixation agents, and provide theoretical guidance for the application of sulfur fixation in the process of coal combustion [20-27].

Experiment and simulation calculation

Experiment introduction

A circulating fluidized bed boiler in a certain power plant was selected for the experiment, with a rated load of 465 tonne per ourh, and model HG-465/13.7-LWM17. The test equipment selected is Qingdao Laoying 3102H automatic flue gas tester. Table 1 is the coal sample and the received basic industrial analysis data after mixing the coal sample and the composite mineralized sulfur-fixing agent according to a certain mass ratio.

It is the preparation method of composite mineralization sulfur fixation agent. After mixing certain raw materials according to the proportion in tab. 2, grind them into small particles of about 0.5 mm with a mill. The composition of the composite mineralization sulfur stabilizer is rich in nature. The materials can choose slag, bauxite*, etc.* Under the action of high temperature and accelerator, the calcium and aluminum groups can react with sulfur to form the compound calcium sulfoaluminate which is very stable under high temperature conditions.

Table 1. Proximate analysis of coal and fixing sulfur agent

Sample	Total sulfur [%]	Flee moisture [%]	Internal moisture [%]	Ash content [%]	Volatile matter [%]	Fixed carbon [%]	Calorific value [kJkg^{-1}]
Mixed sample of coal and sulfur fixing agent	0.51	8.2	1.21	38.14	17.77	42.88	20448
Coal sample	0.49	6.0	1.22	34.30	23.07	41.41	19117

Table 2. Main component of fixing sulfur agent

Mass percent [%]			
CaO	Al_2O_3	Fe_2O_3	CaF_2
50	40	7	3

The Fe_2O_3 and CaF_2 as accelerators can improve the chemical activity of the reaction, reduce the activation energy of the reaction, and improve the sulfur fixation efficiency of the composite mineralized sulfur fixation agent:

– The formation reaction of $CaSO_4$.

The SO_2 precipitated in the coal reacts with CaO to form sulfate, namely:

$$2CaO + 2SO_2 + O_2 \rightarrow 2CaSO_4$$

– Formation reaction of calcium sulfoaluminate.

The $CaSO_4$ is an important part of sulfur fixation products, and its stability is also very important. Under high temperature conditions, especially in the presence of calcium fluoride, $CaSO_4$ is easy to decompose to form sulfur oxides and calcium-based compounds, reducing the desulfurization efficiency. In order to prevent it from decomposing, it is necessary to perform a resolidification reaction on the generated $CaSO_4$ to generate calcium sulfoaluminate that is stable under high temperature conditions and ensure the desulfurization efficiency in the furnace.

$$CaO + Al_2O_3 \rightarrow CaO\cdot Al_2O_3$$

$$3(CaO\cdot Al_2O_3) + CaSO_4 \rightarrow 3CaO\cdot 3Al_2O_3\cdot CaSO_4$$

$$3CaO + 3Al_2O_3 + CaSO_4 \rightarrow 3\ CaO\cdot 3Al_2O_3\cdot CaSO_4$$

In the reaction, the sulfur-fixing agents are CaO, Al_2O_3, and the accelerators are Fe_2O_3, CaF_2, which promote the formation of calcium sulfoaluminate.

Calculation principle

Calculation method and theory

In this paper, the CASTEP module of materials studio platform is used to optimize and simulate the structure of $CaCO_3$, CaO, $CaSO_4$, and calcium sulfoaluminate. The research is based on density functional theory, super soft pseudopotential plane wave method, and pseudopotential instead of ion potential, using the plane wave basis set to expand the wave function of the orbit for optimization. The most important step of this research is to solve the Kohn-Sham equation simplified by density functional theory [28-30]:

$$h_{\mathrm{ks}}\varphi_i(r) = \left[-\frac{\nabla}{2} - \sum \frac{Z_q}{|r - R_q|} + \int \frac{\rho(r)}{|r - r'|}\mathrm{d}r' + V_{XC}\right]\varphi_i(r) \tag{1}$$

where h_{ks} is the Hamiltonian in the K-S equation, $-\nabla/2$ is the electronic kinetic energy, $-\sum z_q/|r - R_q|$ represents the positional potential energy of the electron and each nucleus, $\int\rho(r)/|r - r'|\mathrm{d}r'$ represents the interaction term of the potential energy between the electrons, which is the Hatree potential energy phase, V_{XC} – the functional derivative of the exchange correlation energy, and $\varphi_i(r)$ – the wave function of a single electron:

$$\rho(r) = \sum_i n_i \left|\varphi_i(r)\right|^2 \tag{2}$$

where $\rho(r)$ is the electron density, n_i – the occupancy number, and $\varphi_i(r)$ – the wave function of a single electron:

$$E_x^{GGA} = E_x^{LDA} - \sum_\sigma F\left(x_\sigma\right)\rho_\sigma^{4/3}(r)\,\mathrm{d}r \tag{3}$$

where E_x^{GGA} is expressed as the generalized gradient approximation, E_x^{LDA} – the local density approximation (LDA), and $F(x_\sigma)\rho_\sigma^{4/3}$ – the gradient:

$$E_{xc}^{\mathrm{LDA}}[\rho] = E_x^{\mathrm{LDA}}[\rho] + E_c^{\mathrm{LDA}}[\rho] = \int \varepsilon_x[\rho]\rho(r)\,\mathrm{d}r + \int \varepsilon_c[\rho]\rho(r)\,\mathrm{d}r \tag{4}$$

where $E_{xc}^{\mathrm{LDA}}[\rho]$ is expressed as the exchange correlation energy of electrons, $\varepsilon_x[\rho]$ and $\varepsilon_c[\rho]$ are, respectively, expressed as exchange energy density function and correlation energy density function.

According to the aforementioned equations, the spatial structure of these four minerals are geometrically optimized to obtain the most stable structure of each mineral. In the geometric optimization calculation, in order to ensure that the geometric optimization is close to the real structure, some specific parameters need to be set. In order to select a finite plane wave number, the cutoff energy was set to 350 eV, the single atom convergence standard of the system was set to $1.0 \cdot 10^{-5}$ eV. In order to ensure that the calculation is carried out under periodic boundary conditions, the crystal unit cells of 4 minerals are selected, and the k points of the Brillouin zone are selected as shown in tab. 3.

Table 3. The parameters of different mineral

Mineralization	Space group	Crystal face angle [°]			Lattice constant [Å]			Single atom convergence criterion	Truncation energy	*k*-point
		α	β	γ	a	b	c	eV	eV	
$CaSO_4$	BMMB	90	90	90	6.991	6.999	6.240	$1.0 \cdot 10^{-5}$	350	6×5×2
CaO	FM-3M	90	90	90	4.990	4.990	4.990	$1.0 \cdot 10^{-5}$	350	2×3×1
$CaCO_3$	R-3C	90	90	120	4.993	4.993	16.917	$1.0 \cdot 10^{-5}$	350	6×5×2
$3CaO{\cdot}3Al_2O_3{\cdot}CaSO_4$	I23	90	90	90	9.190	9.190	9.190	$1.0 \cdot 10^{-5}$	350	6×6×4

The ground state charge density and phonon-frequency distribution can be obtained by self-consistent iterative calculation. According to the state density of phonon-s, the thermodynamic properties of these four minerals are obtained.

The influence of lattice resonance (temperature) on crystal free energy G:

$$G(T) = E_{\mathrm{tot}} + \frac{1}{2}\int F(\omega)h\omega\,\mathrm{d}\omega + kT\int F(\omega)\ln\left[1 - \exp\frac{h\omega}{kT}\right]\mathrm{d}\omega \tag{5}$$

The effect of temperature on entropy:

$$S(T)=k\left\{\int\frac{\frac{h\omega}{kT}}{\exp\left(\frac{h\omega}{kT}\right)-1}F(\omega)\mathrm{d}\omega-\int F(\omega)\ln\left[1-\exp\frac{h\omega}{kT}\right]\mathrm{d}\omega\right\} \tag{6}$$

The influence of temperature *vs.* heat capacity:

$$C_v(T)=k\int\frac{\left(\frac{h\omega}{kT}\right)^2\exp\left(\frac{h\omega}{kT}\right)}{\left[\exp\left(\frac{h\omega}{kT}\right)-1\right]^2}F(\omega)\mathrm{d}\omega \tag{7}$$

$$C_p=C_v+\alpha^2BVT \tag{8}$$

$$H=G+TS \tag{9}$$

where F is the free energy, E_{tot} – the lattice equilibrium energy, h – the Planck's constant, ω – the lattice wave frequency, k – the Boltzmann's constant, T – the temperature, α – the linear thermal expansion coefficient, and B – the volume modulus of elasticity.

Model construction and optimization

The $CaCO_3$ belongs to the trigonal crystal system, its space group is R-3C, the crystal face angle is $\alpha = \beta = 90°$, $\gamma = 120°$, $a = b = 4.993$ Å, $c = 16.917$ Å. CaO belongs to the cubic crystal system, its space group is FM-3M, the crystal face angle is $\alpha = \beta = \gamma = 90°$, $a = b = c = 4.99$ Å. The $CaSO_4$ belongs to the orthorhombic crystal system, and its space group is CMCM, $\alpha = \beta = \gamma = 90°$, $a = 6.991$ Å, $b = 6.999$ Å, $c = 6.24$ Å. Calcium sulphoaluminate belongs to cubic crystal system, its space group is I23, and its crystal face angle is $\alpha = \beta = \gamma = 90°$, $a = b = c = 9.19$ Å. The single atom convergence standard, truncation energy and k-point of minerals are shown in tab. 3. After the model was built, the 3-D structure of the unit cell was optimized, fig. 1 shows the crystal structure of $CaCO_3$, fig. 2 shows the crystal structure of CaO, fig. 3 shows the crystal structure of $CaSO_4$, and fig. 4 shows the crystal structure of calcium sulfoaluminate.

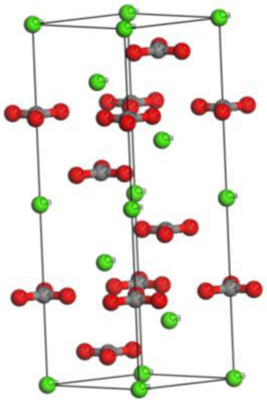

Figure 1. The 3-D structure of $CaCO_3$

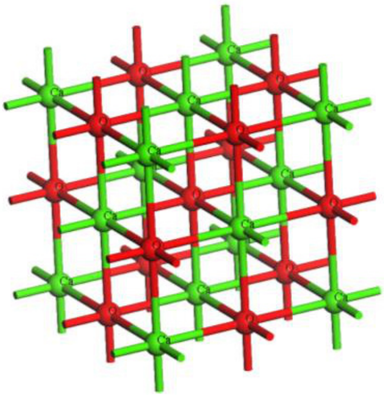

Figure 2. The 3-D structure of CaO

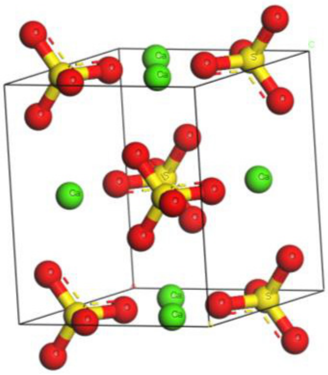

Figure 3. The 3-D structure of $CaSO_4$

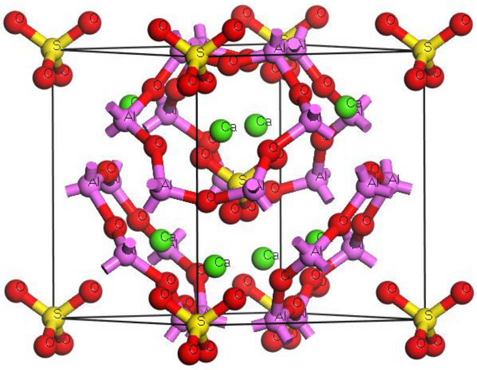

Figure 4. The 3-D structure of $3CaO·3Al_2O_3·CaSO_4$

Results and discussion

Analysis of results

It can be seen from fig. 5 that after adding two desulfurizers, the mass concentration of SO_2 in the flue gas gradually decreases with the increase of the Ca/S ratio. As the Ca/S ratio increases, the initial desulfurization efficiency differs greatly, and then the gap gradually narrows, mainly because when the Ca/S ratio increases to a certain level, the desulfurization efficiency of calcium-based sulfur fixer increases little. Adding limestone as a desulfurizer, with the increase of Ca/S, and finally increase to Ca/S = 3.0, it cannot meet the ultra-low emission requirements, and the minimum SO_2 mass concentration in the flue gas can reach about 80 mg/Nm^3. Adding a composite mineralized sulfur-fixing agent as a desulfurizing agent, when Ca/S = 2.5 (3.0), the mass concentration of SO_2 in the flue gas is below 30 mg/Nm^3, which can meet the ultra-low emission requirements. Because of the existence of Fe_2O_3, CaF_2 and other accelerants, the intermediate products $Ca_4Al_2Fe_2O_{10}$, $Ca_2Al_2SiO_7$, and Ca_2SiO_4 in the formation process of calcium sulphoaluminate encapsulate the generated $CaSO_4$ and inhibit the high temperature decomposition of $CaSO_4$. In addition, on the basis of one-time sulfur fixation generate $CaSO_4$, it continues to react with aluminum bases to form calcium sulfoaluminate that is difficult to decompose at high temperatures, which not only prevents the decomposition of $CaSO_4$, but also forms a new calcium sulfoaluminate phase, ensuring sulfur fixation effect.

It can be seen from fig. 6 that when an appropriate amount of limestone powder (Ca/S = 2.5) is sprayed into the circulating fluidized bed furnace, the mass concentration of SO_2 in the flue gas is unstable in the first five hours, mainly because the limestone is sprayed into the furnace. Decomposition in the furnace requires time and has a certain lag. With the passage of time, the SO_2 concentration is basically stable, and the maximum is basically not more than 100 mg/Nm^3. After the coal (Ca/S = 2.5) added with the composite mineralized sulfur-fixing agent is burned, the SO_2 mass concentration is unstable in the first four hours, and then basically maintained at a low position (<30 mg/Nm^3). The wave amplitude is very small, mainly because the composite mineralization sulfur fixer and coal are uniformly mixed and enter the furnace at the same time. At the same calcium-sulfur ratio (Ca/S = 2.5), the SO_2 concentration of limestone added is about three times that of composite mineralized sulfur-fixing agent.

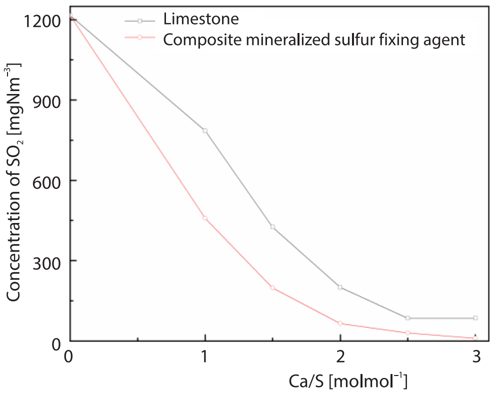

Figure 5. Concentration of SO_2 changes along with Ca/S

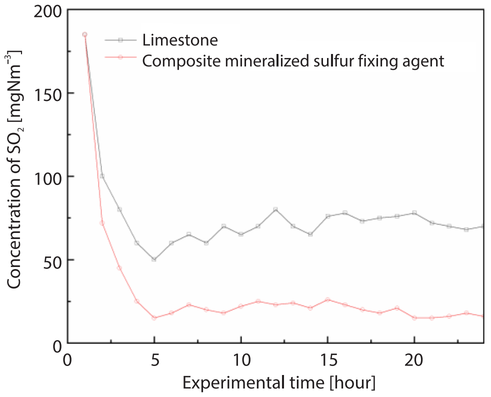

Figure 6. Concentration of SO_2 changes along with time

Thermodynamic analysis

According to the first principles, $CaCO_3$, CaO, $CaSO_4$ and calcium sulphoaluminate are optimized. After the stable structures are obtained by geometric optimization, the ground state charge density is calculated, and then the phonon-frequency distribution and phonon-state density are obtained by self-consistent iteration. The thermodynamic properties of these four minerals can be obtained. The calculation of the thermodynamic properties of these four minerals were carried out under one atmosphere, with the thermodynamic temperatures ranging from 25-1000 K, and a set of data was recorded every 25 K. According to the calculation results, find out the enthalpy, H, entropy, TS, heat capacity, C_p, and Gibbs free energy, G, of the four minerals as a function of temperature, see figs. 7-10. In the entire temperature range (25~1000 K), the TS, constant pressure C_p, and H of the four minerals all increase with the increase of temperature, while the G decreases with the increase of temperature. It conforms to the laws of thermodynamics.

Figures 7 and 8 show that the enthalpy and entropy of the four minerals show an upward trend with temperature. Before 150 K, the enthalpy and entropy of the four minerals have little difference. As the temperature rises, the enthalpy and entropy of the four minerals have little difference. The enthalpy and entropy increase rapidly, and the difference between enthalpy

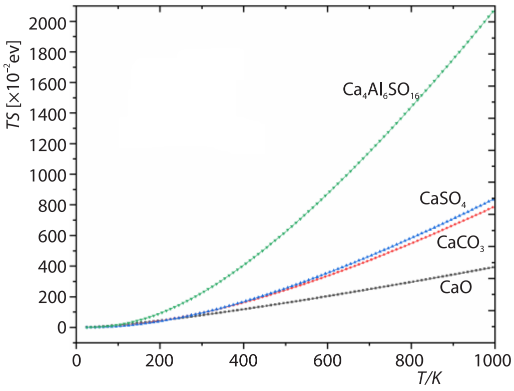

Figure 7. The change of entropy value along with temperature

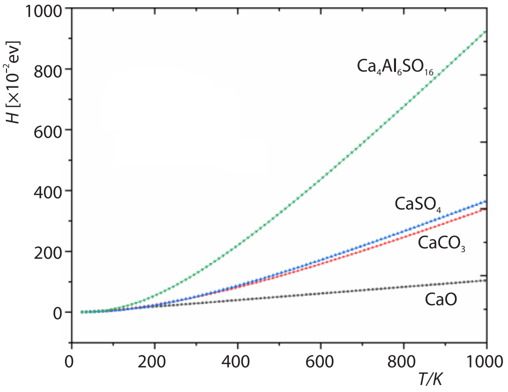

Figure 8. The change of enthalpy value along with temperature

and entropy is larger, indicating that more energy is needed to decompose calcium sulfoaluminate, and calcium sulfoaluminate is more stable.

The enthalpy and entropy of CaO increase very slowly, and the difference in enthalpy and entropy is small, indicating that it takes very little energy to decompose CaO, and CaO is more likely to participate in the reaction. The increasing trend of enthalpy and entropy of $CaCO_3$ and $CaSO_4$ is between them, and their stability is between them. The enthalpy and entropy values of $CaSO_4$ are slightly higher than those of $CaCO_3$, indicating that $CaSO_4$ is more stable than $CaCO_3$. The generation of $CaSO_4$ requires the decomposition of $CaCO_3$, so it takes more time than the reaction of CaO.

As shown in fig. 9, the specific heat capacity at constant pressure of the four minerals all increased with the increase of temperature. The specific heat capacity at constant pressure of calcium sulfoaluminate is higher than that of the other three minerals in the whole temperature range. The specific heat capacity at constant pressure of CaO is the lowest in hot melting, and the specific heat capacity of $CaCO_3$ and $CaSO_4$ is between them. Before 400 K, the specific heat capacity of calcium sulfoaluminate changes drastically, and then gradually become flat, indicating that at low temperatures, calcium sulfoaluminate absorbs more heat. As the temperature rises, the heat absorption begins to decrease. Before 150 K, the specific heat capacity of $CaCO_3$ at constant pressure is higher than that of $CaSO_4$ at constant pressure, indicating that $CaCO_3$ has more heat absorption at low temperature. After 150 K, $CaSO_4$ has more heat absorption, but the constant pressure hot melting of $CaSO_4$ and $CaCO_3$ have little change.

Figure 10 shows that the Gibbs free energy of the four minerals decreases with increasing temperature. Before 150 K, the Gibbs free energy of the four minerals is almost the same. After 150 K, the change of Gibbs free energy of CaO is very small, and the change of Gibbs free energy of calcium sulphoaluminate is very sharp. The Gibbs free energy of $CaCO_3$ and $CaSO_4$ is between them. Between 150 K and 600 K, the Gibbs free energy of $CaCO_3$ and $CaSO_4$ is almost the same. After 600 K, the Gibbs free energy of $CaCO_3$ is always greater than that of $CaSO_4$. It shows that before the temperature is lower than 600 K, $CaCO_3$ decomposes very little, and the $CaSO_4$ is also very small, it is mainly calcium sulfoaluminate.

Using the simulated data based on the principle of quantum mechanics, the trend of each thermodynamic quantity with temperature change is compared by drawing, which provides a theoretical basis for the removal of sulfur from coal in industrial applications.

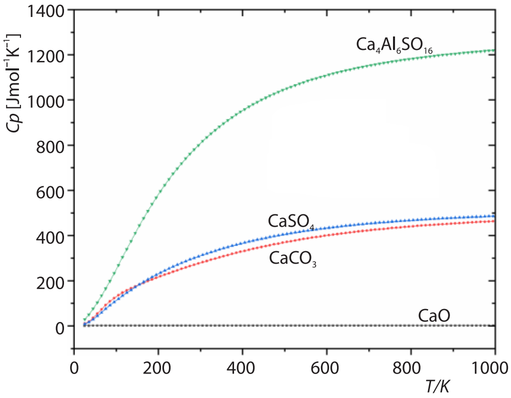

Figure 9. The change of specific heat capacity value along with temperature

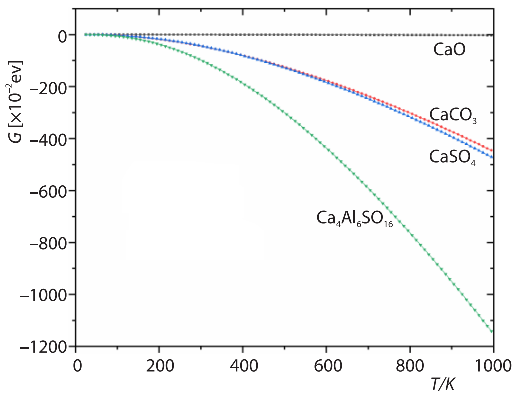

Figure 10. The change of Gibbs free energy value along with temperature

Energy band structure and density of states analysis

Energy band and density of states analysis of CaO

It can be seen from fig. 11(a) that the valence band of CaO is divided into four zones: a group of valence bands ($1^{\#}$ band) near –37.5 eV, a group of valence bands ($2^{\#}$ band) near –19eV, a group of valence bands ($3^{\#}$ band) near –15 eV, and a group of valence bands ($4^{\#}$ band) below 0 eV. According to the comprehensive analysis of figs. 11(b)-11(d), $1^{\#}$ valence band mainly includes the 3S orbital contribution of Ca, $2^{\#}$ valence band mainly includes the 3p orbital contribution of Ca and the 2s orbital contribution of a small amount of O, $3^{\#}$ valence band mainly includes the 2s orbital contribution of O and the 3p orbital contribution of a small amount of Ca, and $4^{\#}$ valence band mainly includes the 2p orbital contribution of O, the 3d orbital contribution of a small amount of Ca. Therefore, the top of the valence band is mainly contributed by the 2p orbital of O, and the bottom of the conduction band is mainly contributed by the 3d orbital of Ca; the Ca ions involved in the reaction easily react with sulfur-containing substances to generate calcium sulfite or $CaSO_4$.

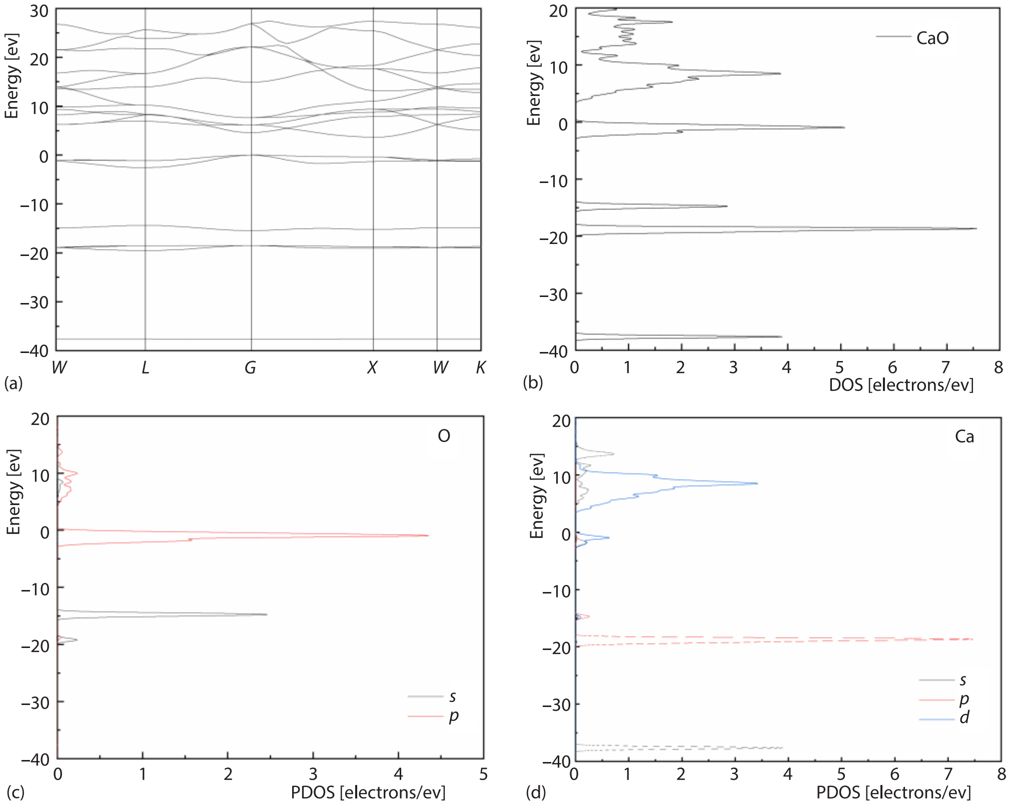

Figure 11. The CaO energy band structure and density of states diagram; (a) CaO energy band structure, (b) CaO total density of states, (c) O partial density of states, and (d) Ca partial density of states

Analysis of energy band and density of states of $CaCO_3$

It can be seen from fig. 12(a) that the valence band of $CaCO_3$ is divided into four zones: a group of valence bands ($1^\#$ band) near –38eV, a group of valence bands (2 # band) near –21 eV, a group of valence bands ($3^\#$ band) near –19 eV, a group of valence bands (4 # band) near –7 eV, and a group of valence bands ($5^\#$ band) below 0 eV. According to the comprehensive analysis of fig. 11(b)-11(d), $1^\#$ valence band mainly includes the 3s orbital contribution of Ca, $2^\#$ valence band mainly includes the 2s orbital contribution of C and the 2s orbital contribution of O, $3^\#$ valence band mainly includes the 3p orbital contribution of Ca and a small amount of 2p orbital contribution of C and 2s orbital contribution of O, $4^\#$ valence band

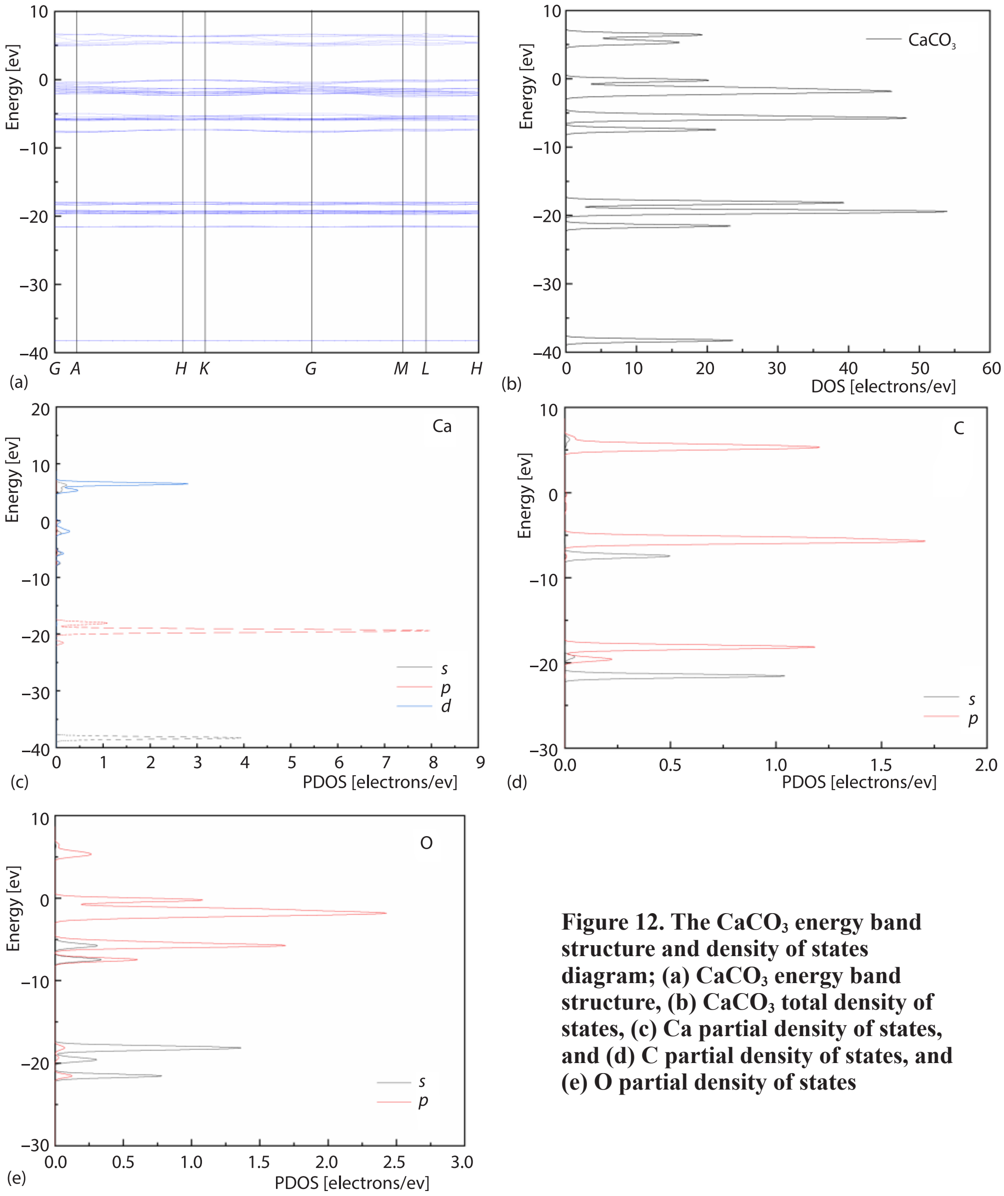

Figure 12. The $CaCO_3$ energy band structure and density of states diagram; (a) $CaCO_3$ energy band structure, (b) $CaCO_3$ total density of states, (c) Ca partial density of states, and (d) C partial density of states, and (e) O partial density of states

mainly includes the 2p orbital contribution of O and the 2p orbital contribution of C, and $5^{\#}$ valence band mainly includes the 2p orbital contribution of O and the 3d orbital contribution of a small amount of Ca. Therefore, the top of the valence band mainly has the 2p orbital contribution of O, and the bottom of the conduction band mainly has the 3d orbital contribution of Ca, the 2p orbital contribution of part of C, and the 2p orbital contribution of a small amount of O. The Ca ions involved in the reaction easily react with sulfur-containing substances. However, due to the C element on the conduction band, the C must be reacted before it can react with Ca. Therefore, the reaction speed is significantly slower than that of CaO.

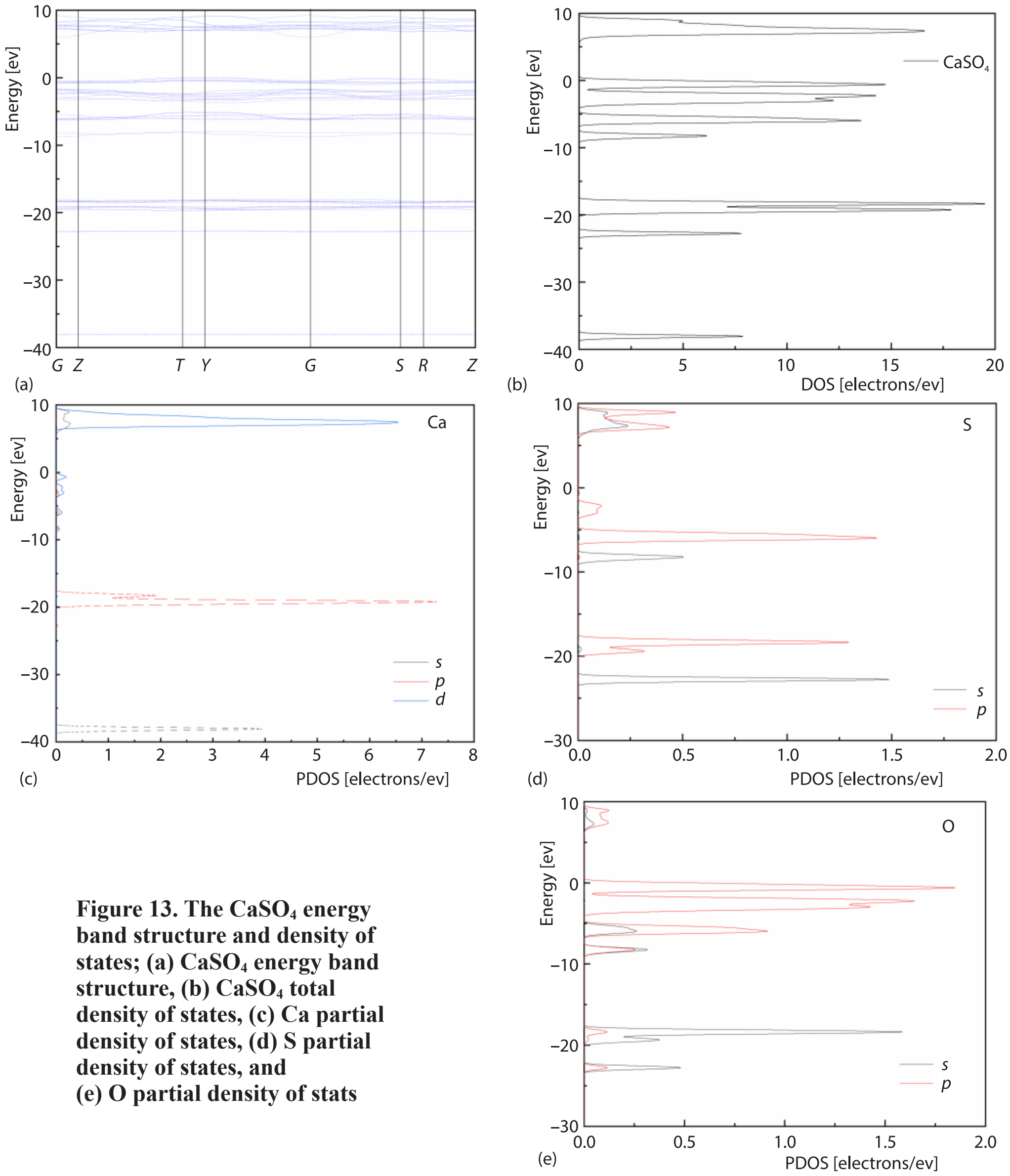

Figure 13. The $CaSO_4$ energy band structure and density of states; (a) $CaSO_4$ energy band structure, (b) $CaSO_4$ total density of states, (c) Ca partial density of states, (d) S partial density of states, and (e) O partial density of stats

It can be seen from fig. 13(a) that the valence band of $CaSO_4$ is divided into four zones. There is a set of valence bands near –38eV (1$^{\#}$ valence band), and a set of valence bands near –23eV (2# valence band), and near –19eV. There is a set of price bands (3$^{\#}$ price band), a set of price bands near –8eV (4$^{\#}$ price band), and a set of price bands below 0eV (5$^{\#}$ price band). According to the comprehensive analysis of figs. 13(b)-13(e), 1$^{\#}$ valence band mainly includes the 3s orbital contribution of Ca, 2$^{\#}$ valence band mainly includes the 3s

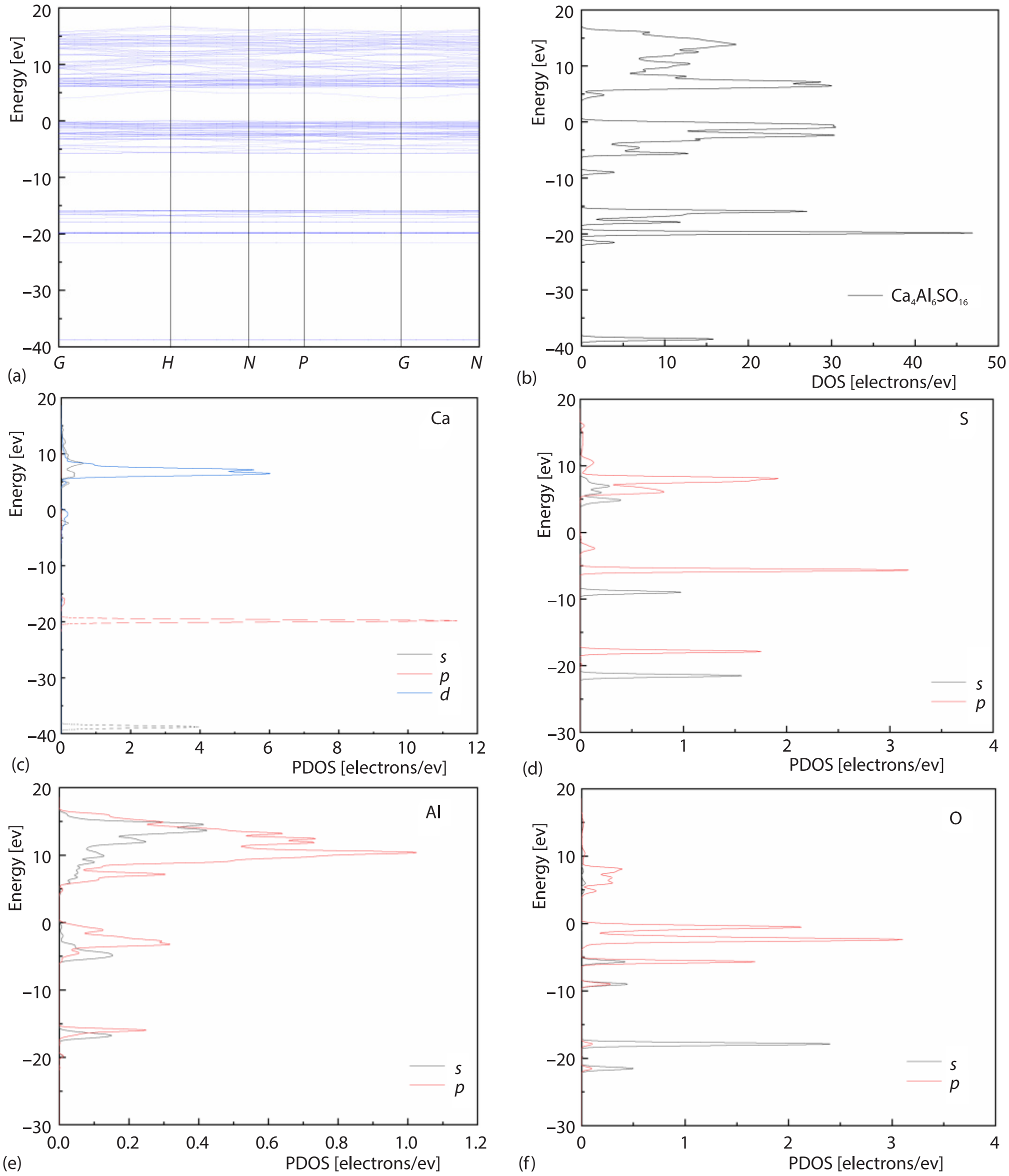

Figure 14. The $3CaO\cdot 3Al_2O_3\cdot CaSO_4$ energy band structure and density of states; (a) $3CaO\cdot 3Al2O_3\cdot CaSO_4$ energy band structure diagram, (b) $3CaO\cdot 3Al_2O_3\cdot CaSO_4$ total density of states, (c) Ca partial density of states, (d) S partial density of states, (e) Al partial density of states, and (f) O partial density of states

orbital contribution of S and the 2s orbital contribution of O, $3^{\#}$ valence band mainly includes the 3p orbital contribution of Ca and a small amount of 3p orbital contribution of S and the 2s orbital contribution of O, $4^{\#}$ valence band mainly includes the 2p orbital contribution of O and the 3s orbital contribution of S, and $5^{\#}$ valence band mainly includes the 3p orbital contribution of Ca and a small amount of 3p orbital contribution of S and the 2s orbital contribution of O. The 2p orbital contribution of S and the 3d orbital contribution of a small amount of Ca.

Therefore, the top of the valence band is mainly contributed by the 2p orbital of O and a small amount of 3p orbital of S, while the bottom of the conduction band is mainly contributed by the 3d orbital of Ca, the 3p orbital of some S and a small amount of 2p orbital of O. The stable compounds were formed by the reaction of Ca with sulfur.

It can be seen from fig. 14(a) that the calcium sulphoaluminate valence band is divided into four zones: there is a set of valence bands ($1^{\#}$ valence band) around –38 eV, a set of valence bands ($2^{\#}$ valence band) around –22 eV, a set of valence bands (3# valence band) around -20eV, a set of valence bands (4# valence band) around –17 eV, and a set of valence bands ($5^{\#}$ valence band) around –7eV. There is a group of valence bands below 0 eV (valence band $6^{\#}$). According to the comprehensive analysis of figs. 14(b)-14(f), $1^{\#}$ valence band is mainly composed of 3s orbital contribution of Ca, $2^{\#}$ valence band is mainly composed of 3s orbital contribution of S and 2s orbital contribution of O, $3^{\#}$ valence band is mainly composed of 3p orbital contribution of Ca and a small amount of 3p orbital contribution of S and 2s orbital contribution of O, $4^{\#}$ valence band is mainly composed of 2s orbital contribution of O, 3p orbital contribution of S and 3s and 3p orbital contribution of Al, and $5^{\#}$ valence band is mainly composed of O and 3p orbital contribution of O. The 2p orbital contribution of S and the $6^{\#}$ valence band are mainly O 2p orbital contribution, Al 3p orbital contribution and a small amount of S 3p orbital contribution. Therefore, at the top of the valence band there are mainly 2p orbital contributions of O and a small amount of 3p orbital contributions of S and Al, while at the bottom of the guide band, there are mainly 3d orbital contributions of Ca, 3s and 3p orbital contributions of part of S, 3p orbital contributions of a small amount of Al and 2p orbital contributions of O. Elements Ca and S, Al, O form stable compounds.

Conclusions

- The main components of the compound mineralization sulfur fixation agent are CaO and Al_2O_3. When the ratio of calcium to sulfur reaches 2.5, the desulfurization efficiency is more than 95%.
- The thermodynamic values of $CaCO_3$, CaO, $CaSO_4$, calcium sulfoaluminate and products are obtained by the first principles calculation method. Calcium sulfoaluminate has high stability, and CaO is the easiest to react. The $CaCO_3$ is relatively stable at low temperature, and will decompose slowly after the temperature is higher than 600 K. With the increase of temperature, it is conducive to the formation of calcium-based products.

Acknowledgment

The authors appreciate the support of the Innovative Research Team of Henan Polytechnic University (T2020-3) and the National Natural Science Foundation of China (No. 51774115).

References

[1] Sarbassov, Y., *et al.*, The SO_3 Formation and the Effect of Fly Ash in a Bubbling Fluidised Bed under Oxy-Fuel Combustion Conditions, *Fuel Processing Technology*, *167* (2017), Dec., pp. 314-321

[2] Jin, D. S., *et al.*, Simultaneous Removal of SO_2 and NO by Wet Scrubbing Using Aqueous Chlorine Dioxide Solution, *Journal of Hazardous Materials*, *135* (2006), 1-3, pp. 412-417

[3] Zhou, G. M., *et al.*, Application Research of SNCR Technology in the Pulverized-Coal Fired Boiler, *Power System Engineering*, *26* (2010), pp. 18-21

[4] Weirong, G. U., *et al.*, Technology Status and Analysis on Coal-Fired Flue Gas Denitrification, *Chemical Industry and Engineering Progress*, *31* (2012), 9, pp. 2084-2092

[5] Zhang, J., *et al.*, Control Technologies and Evaluation of Mercury in Flue Gas of Waste Incineration, *Environmental Sanitation Engineering*, *20* (2012), pp. 34-36

[6] Zhang, B., *et al.*, Increasing Oxygen Functional Groups of Activated Carbon with Non-Thermal Plasma to Enhance Mercury Removal Efficiency for Flue Gases, *Chemical Engineering Journal*, *263* (2015), Mar., pp. 1-8

[7] Zhao, W., Wu, Z., Simultaneous Absorption of NO and SO_2 by FeIIEDTA Combined with Na_2SO_3 Solution, *Chemical Engineering Journal*, *132* (2007), 1-3, pp. 227-232

[8] Bricl, M., Avsec, J., Design of Thermal Power Plant Modernization & Rehabilitation Model for the Newmarket Demands and Challenges, *Thermal Science*, *21* (2021), 4A, pp. 2701-2711

[9] Shimizu, T., *et al.*, Capture of SO_2 by Limestone in a 71 MWe Pressurized Fluidized Bed Boiler, *Thermal Science*, *7* (2003), 1, pp. 17-31

[10] Smajevic, I., *et al.*, Co-firing Bosnian Coals with Woody Biomass: Experimental Studies on a Laboratory-Scale Furnace and 110 MWe Power Unit, *Thermal Science*, *16* (2012), 3, pp. 789-804

[11] Zhao, Y., *et al.*, Experimental Study on Simultaneous Desulfurization and Denitrification Based on Highly Active Absorbent, *Journal of Environmental Sciences*, *18* (2006), 2, pp. 281-286

[12] Chiu, C. H., *et al.*, Multipollutant Control of Hg/SO_2/NO from Coal-Combustion Flue Gases Using Transition Metal Oxide-Impregnated SCR Catalysts, *Catalysis Today*, *245* (2015), May, pp. 2-9

[13] Zhang, S., *et al.*, Integrated Removal of NO and Mercury from Coal Combustion Flue Gas Using Manganese Oxides Supported on TiO_2, *Journal of Environmental Sciences*, *53* (2017), 003, pp. 141-150

[14] Zhang, S., *et al.*, Enhancement of CeO_2 Modified Commercial SCR Catalyst for Synergistic Mercury Removal from Coal Combustion Flue Gas, *RSC Advances*, *10* (2020), 42, pp. 25325-25338

[15] Guo, S., *et al.*, Simultaneous removal of SO_2 and NO_x with Ammonia Combined with Gas-Phase Oxidation of NO Using Ozone, *Chemical Industry and Chemical Engineering Quarterly*, *21* (2015), 2, pp. 305-310

[16] Zheng, Y., *et al.*, Review of Technologies for Mercury Removal from Flue Gas from Cement Production Processes, *Progress in Energy and Combustion Science, 38* (2012), 5, pp. 599-629

[17] Guilin, L. U., *et al.*, First-Principles Calculation of Thermodynamic Properties of XCO_3(X = Ca, Mg), *Materials Review*, *26* (2012), pp. 122-126

[18] Sousa, J., *et al.*, Catalytic Oxidation of NO to NO_2 on N-Doped Activated Carbons, *Catalysis Today*, 176, (2011), 1, pp. 383-387

[19] Jeguirim, M., *et al.*, Interaction Mechanism of NO_2 with Carbon Black: Effect of Surface Oxygen Complexes, *Journal of Analytical & Applied Pyrolysis*, *72* (2004), 1, pp. 171-181

[20] Zhang, W. J., *et al.*, Study of NO Adsorption on Activated Carbons, *Applied Catalysis B Environmental*, *83* (2008), 1-2, pp. 63-71

[21] Liu, D., *et al.*, Utilization of Waste Concrete Powder with Different Particle Size as Absorbents for SO_2 Reduction, *Construction and Building Materials*, *266* (2021), 121005

[22] Yu, H., *et al.*, Dynamic Modelling for SO_2-NO_x Emission Concentration of Circulating Fluidized Bed Units Based on Quantum Genetic Algorithm-Extreme Learning Machine, *Journal of Cleaner Production*, *324* (2021), 129170

[23] Wang, X., *et a*l., Simultaneous SO_2 and NO Removal by Pellets Made of Carbide Slag and Coal Char in a Bubbling Fluidized-Bed Reactor, *Process Safety and Environmental Protection*, *134* (2020), Feb., pp. 83-94

[24] Morselli, G. R., Ando, R. A., The SO_2 Capture by Tricyanomethanide Ionic Liquids: Unraveling Anion-Gas Interactions by Resonance Raman Spectroscopy, *Chemical Physics Letters*, (2021), 139106

[25] YAN, Y.-G., *et al.*, Simultaneous Removal of SO_2, NO_x and HgO by O_3 Oxidation Integrated with Biocharcoal Adsorption, *Journal of Fuel Chemistry and Technology*, *48* (2020), 12, pp. 1452-1460

[26] Ng, K. H., *et al.*, A Review on Dry-Based and Wet-Based Catalytic Sulphur Dioxide (SO_2) Reduction Technologies, *Journal of Hazardous Materials*, *423* (2022), 127061

[27] Li, B., Ma, C., Study on the Mechanism of SO_2 Removal by Activated Carbon, *Energy Procedia*, *153* (2018), Oct., pp. 471-477

[28] Ying, Z., *et al*., First-Principle Theory Calculation of Electronic Structures of Scheelite, Fluorite and Calcite, *Chinese Journal of Rare Metals*, *42* (2014), 12, pp. 3612-3617

[29] Wang, Z. H., *et al.*, Experimental Research for the Simultaneous Removal of NO_x and SO_2 in Flue Gas by O_3, *Zhongguo Dianji Gongcheng Xuebao/Proceedings of the Chinese Society of Electrical Engineering*, *27* (2007), 11, pp. 1-5

[30] Zhang, B., *et al.*, Study on NO Adsorptive Removal on Modified Activated Carbon, *New Chemical Materials*, *43* (2015), 43, pp. 111-113

Paper submitted: August 24, 2021
Paper revised: October 17, 2021
Paper accepted: October 30, 2021